Journal of Neuroimmunology 334 (2019) 576998

Contents lists available at ScienceDirect

Journal of Neuroimmunology

journal homepage: www.elsevier.com/locate/jneuroim

Copper chelation and autoimmunity differentially impact myelin in the hippocampal-prefrontal circuit

Mara Nickel[a], Farida Eid[b], Peter Jukkola[c], Chen Gu[a,c,*]

[a] Department of Biological Chemistry and Pharmacology, The Ohio State University, Columbus, OH 43210, USA
[b] College of Arts and Sciences, The Ohio State University, Columbus, OH 43210, USA
[c] Biomedical Sciences Graduate Program, The Ohio State University, Columbus, OH 43210, USA

ARTICLE INFO

Keywords:
Gray matter myelin
Hippocampus
Prefrontal cortex (PFC)
Cuprizone model
Experimental autoimmune encephalomyelitis (EAE)
Myelin basic protein (MBP)

ABSTRACT

Multiple sclerosis (MS) is an inflammatory demyelinating disease of the central nervous system. About 50% of MS patients develop deficits in learning, memory and executive function, which are accompanied by demyelinating lesions in the hippocampus and/or prefrontal cortex (PFC). Why demyelination in these regions occurs in some patients but not in others and what is the underlying mechanism remain unclear. Here we report that myelin density in the hippocampus and PFC is markedly reduced in the cuprizone model, but not in the chronic experimental autoimmune encephalomyelitis. These two models can be used for studying different neuropathophysiological aspects of demyelinating diseases.

1. Introduction

Proper myelination is vital for various neurophysiological functions of the central nervous system (CNS). Myelin is composed of compacted lipid membranes that wrap around axons, providing trophic support, as well as electrical insulation in saltatory and efficient propagation of action potentials. Disruption to myelin can lead to CNS diseases, including multiple sclerosis (MS). MS is the most common inflammatory demyelinating disease of the CNS, but still has no known origin or cure. MS is likely triggered by environmental factors that act on a genetically susceptible host (Baecher-Allan et al., 2018; Olsson et al., 2017). MS affects not only sensory and motor functions, but also higher-order brain functions. Cognitive deficits occur in about half of MS patients, particularly involving depression, stress, anxiety, and impairment of executive function, memory, attention and mental processing speed (Achiron and Barak, 2003; Gaudino et al., 2001; Jongen et al., 2012; Rao, 1995; Rao et al., 1991). This appears consistent with the fact that hippocampal and cortical demyelinating lesions are frequently observed in MS patients (Geurts et al., 2007; Jongen et al., 2012). On the other hand, myelin reduction has been implicated in cognitive deficits in various neurological and mental disorders, such as schizophrenia, major depressive disorder, bipolar disorder, Alzheimer's disease and posttraumatic stress disorder (PTSD) (Bartzokis et al., 2007; Flynn et al., 2003; Haroutunian et al., 2014; Li et al., 2016; Rajkowska et al., 2015). However, the mechanisms underlying CNS demyelination leading to cognitive deficits remain poorly understood.

To uncover the pathogenic mechanisms of MS and search for treatment strategies, different animal models were developed, including the murine experimental autoimmune encephalomyelitis (EAE) model and the cuprizone model. They represent two major mouse models currently used for studying MS. Although CNS demyelination can be induced in both models, it is through different pathogenic mechanisms. EAE includes an autoimmune response to myelin proteins as the antigen with infiltration of immune cells into the CNS, whereas the cuprizone model relies on ingestion of cuprizone, a copper chelator, that induces apoptosis of oligodendrocytes and hence demyelination (Lassmann and Bradl, 2017; Ransohoff, 2012). Consistent with the link between myelin and cognition, impairments in cognition, spatial working memory and decreased social interaction were observed in the cuprizone model (Serra-de-Oliveira et al., 2015; Xu et al., 2009). Whether cuprizone feeding increases or decreases anxiety-like behaviors remains controversy (Franco-Pons et al., 2007; Serra-de-Oliveira et al., 2015; Xu et al., 2009). In EAE mice, several studies reported anxiety- and depression-like symptoms (Jones et al., 2008; Peruga et al., 2011; Pollak et al., 2002). Thus, these two mouse models likely share some cognitive and behavioral deficits observed in many MS patients.

Many of the behaviors that are altered in MS patients and animal models rely on the proper function of the hippocampus and prefrontal cortex (PFC), which are two interconnected brain regions and play

* Corresponding author at: 182 Rightmire Hall, 1060 Carmack Road, The Ohio State University, Columbus, OH 43210, USA.
E-mail address: gu.49@osu.edu (C. Gu).

https://doi.org/10.1016/j.jneuroim.2019.576998
Received 29 April 2019; Received in revised form 18 June 2019

central roles in higher brain functions, including learning and memory, planning complex cognitive behavior, and moderating social behavior (Nickel and Gu, 2018). The hippocampus, a part of the limbic system, is a paired structure with mirror-image halves in cerebral hemispheres. The hippocampus plays critical roles in spatial memory and in the consolidation of information from short-term memory to long-term memory. Hippocampal neurons carry out these functions by communicating with regions of the cerebral cortex, including the PFC. The PFC is the anterior part of the cerebral cortex in the frontal lobe, and responsible for regulating social and cognitive behavior, planning and decision-making. The hippocampus was thought to be solely responsible for storing new memories, gradually transferring these to the PFC overtime to form remote memory (Frankland and Bontempi, 2005). However, a recent study showed that following initial exposure to a context, both the hippocampus and PFC rapidly form memory cells (Kitamura et al., 2017). Whereas the PFC engram cells become functionally mature with time, allowing the PFC to participate in remote recall, hippocampal engram cells gradually become silent (Kitamura et al., 2017).

Crucial for the computation of neural circuits in the hippocampus and PFC, myelination of the two brain regions is a rather dynamic process and continues well into adulthood (Abraham et al., 2010; Miller et al., 2012; Nickel and Gu, 2018). In addition to the demyelinated lesions in these regions that were observed in patients with neurological disorders such as MS (Nickel and Gu, 2018), social isolation was shown to cause demyelination in both hippocampus and PFC (Eluvathingal et al., 2006; Liu et al., 2012; Makinodan et al., 2012). Widespread demyelination in the brain including corpus callosum, cortex and hippocampus has been documented in the cuprizone model (Dutta et al., 2013; Gudi et al., 2009; Kipp et al., 2017). In the chronic EAE model, several studies reported demyelination in the hippocampus and cortex (Girolamo et al., 2011; Mangiardi et al., 2011; Ziehn et al., 2010), potentially leading to deficits in learning and memory (Aharoni et al., 2019; Sun et al., 2015). Interestingly, it was reported that despite no consistent evidence of chronic loss of layer V neurons in the cortex, there was both reversible and chronic decreases in cortical myelin density in the chronic EAE model (Burns et al., 2014). Therefore, it is of high interest to compare the patterns of demyelination in the hippocampal-prefrontal circuit in the cuprizone and EAE models.

In the present study, we have carefully compared the impacts of copper chelation and autoimmunity on myelination of the hippocampal-prefrontal circuit. Spinal cord and the brain of each mouse were embedded together and included on the same slide after sectioning. Demyelination in white matter (WM) of corpus callosum or spinal cord was clearly observed in cuprizone-fed or EAE mice, respectively. However, whereas myelin density markedly reduced in the hippocampus and PFC in the cuprizone model, we surprisingly observed no clear change of myelin density in the EAE model. Thus, cuprizone and EAE models differentially affect myelin density of the hippocampal-prefrontal circuit and can be used to study different neuropathophysiological aspects of MS.

2. Materials and methods

2.1. Induction of the cuprizone model

All animal experiments were conducted in accordance with the NIH Animal Use Guidelines and approved (2008A0177-R3) by Institutional Animal Care and Use Committee (IACUC) of the Ohio State University. The cuprizone model was established with C57BL/6 mice (8–12 weeks old, both male and female mice purchased from the Jackson Laboratory). The mice were fed with 0.2% cuprizone-containing chow for 5 weeks, followed with another two weeks of regular chow. The mice were perfused and fixed for immunohistochemistry studies at two time points: (1) after 5 weeks of the cuprizone diet as “cuprizone peak,” and (2) after additional 2 weeks of regular chow as “cuprizone recovery.” In our study, we did not observe any difference at myelination, demyelination and remyelination stages between male and female mice, consistent with early studies (Taylor et al., 2010). Thus, we used both male and female mice in the cuprizone model in this study. Any mice that reached 30% weight loss were euthanized immediately and excluded from the study.

2.2. The MOG-induced EAE model

C57BL/6 mice (8–12 week females from the Jackson Laboratory) were used to induce chronic monophasic EAE, as we previously described (Jukkola et al., 2012; Jukkola et al., 2013; Jukkola et al., 2017). In brief, myelin oligodendrocyte glycoprotein (MOG) peptide 35–55 (1 mg/mL) was emulsified in sterile-filtered PBS and Complete Freund's Adjuvant (CFA) containing 2 mg/mL ground inactivated mycobacteria tuberculosis H37Ra. Mice were immunized with 100 μL of MOG/CFA or CFA only (as negative control) by flank subcutaneous injections. Pertussis toxin was administered via tail vein injection at 0 and 2 days post immunization (DPI). Disease progression was monitored daily, and assigned a clinical scoring on a scale of 0–6 [0 = no symptoms, 1 = loss of tail tone, 2 = hindlimb paresis, 3 = moderate paralysis, 4 = paraplegia (complete hindlimb paralysis), 5 = quadriplegia, 6 = death or moribund state]. Grade 6 mice were removed from the study. Mice were sacrificed for immunohistochemistry at appropriate experimental time points. Myelin oligodendrocyte glycoprotein (MOG) peptide 35–55 (MEVGWYRSPFSRVVHLYRNGK) was purchased from Pro-Spec (Rehovot, Israel). Ground inactivated mycobacteria tuberculosis H37Ra and Incomplete Freund's Adjuvant were from Difco Laboratories (Detroit, MI, USA).

2.3. Cardiac perfusion, and tissue fixation and sectioning

Mouse tissues were collected and processed according to previously published methods (Jukkola et al., 2012; Jukkola et al., 2013; Jukkola et al., 2017). Mice were anesthetized with avertin and perfused through the left ventricle of the heart with 20–30 mL ice-cold PBS, followed by 20 mL 4% formaldehyde in PBS (FA/PBS). After carefully removing the brain and spinal cord, the tissues were post-fixed for 1 h in 4% FA/PBS. Following post-fixation, the tissues were cryoprotected in 30% sucrose for at least 24 h and cut into 3-mm blocks using an acrylic brain matrix (Braintree Scientific, Braintree, MA, USA). These sections were embedded in optimal cutting temperature (OCT) media (Sakura Finetek USA, Inc., Torrance, CA, USA) and stored at −80 °C until sectioning. The tissue blocks were cut into 40-μm sections using a Microm HM550 cryostat (Thermo Scientific, Waltham, MA, USA) and mounted on Superfrost Plus microscope slides (FisherScientific, Pittsburgh, PA, USA) for storage at −20 °C.

2.4. Immunostaining of sections of brain and spinal cord

The following antibodies were used in our study: goat polyclonal anti-GFAP (AbCAM, MA, USA), rabbit polyclonal anti-neurofilament 200 antibody (Sigma, MO, USA), rat monoclonal anti-MBP antibody (Chemicon, CA, USA), rabbit polyclonal anti-IBA1 antibody (Waco, VA, USA), rabbit polyclonal anti-cannabinoid receptor-1 antibody (Alomone, Jerusalem), and Cy2-, Cy3-, and Cy5-conjugated secondary antibodies (Jackson ImmunoResearch Laboratories, West Grove, PA, USA). Mouse brain sections were stained according to previously published methods (Barry et al., 2014; Gu et al., 2017; Jukkola et al., 2012; Jukkola et al., 2013; Jukkola et al., 2017). Briefly, sections were permeabilized for 1 h in PBS/1% Triton X-100 at room temperature (RT). The sections were then blocked with 2.5% normal donkey serum in PBS/0.02% Triton X-100 for 1 h at RT, and incubated with the appropriate concentration of primary antibodies in blocking solution overnight at 4 °C. The sections were washed 5 × 5 min using PBS/0.02% Triton X-100, and incubated for 3 h with secondary antibodies in

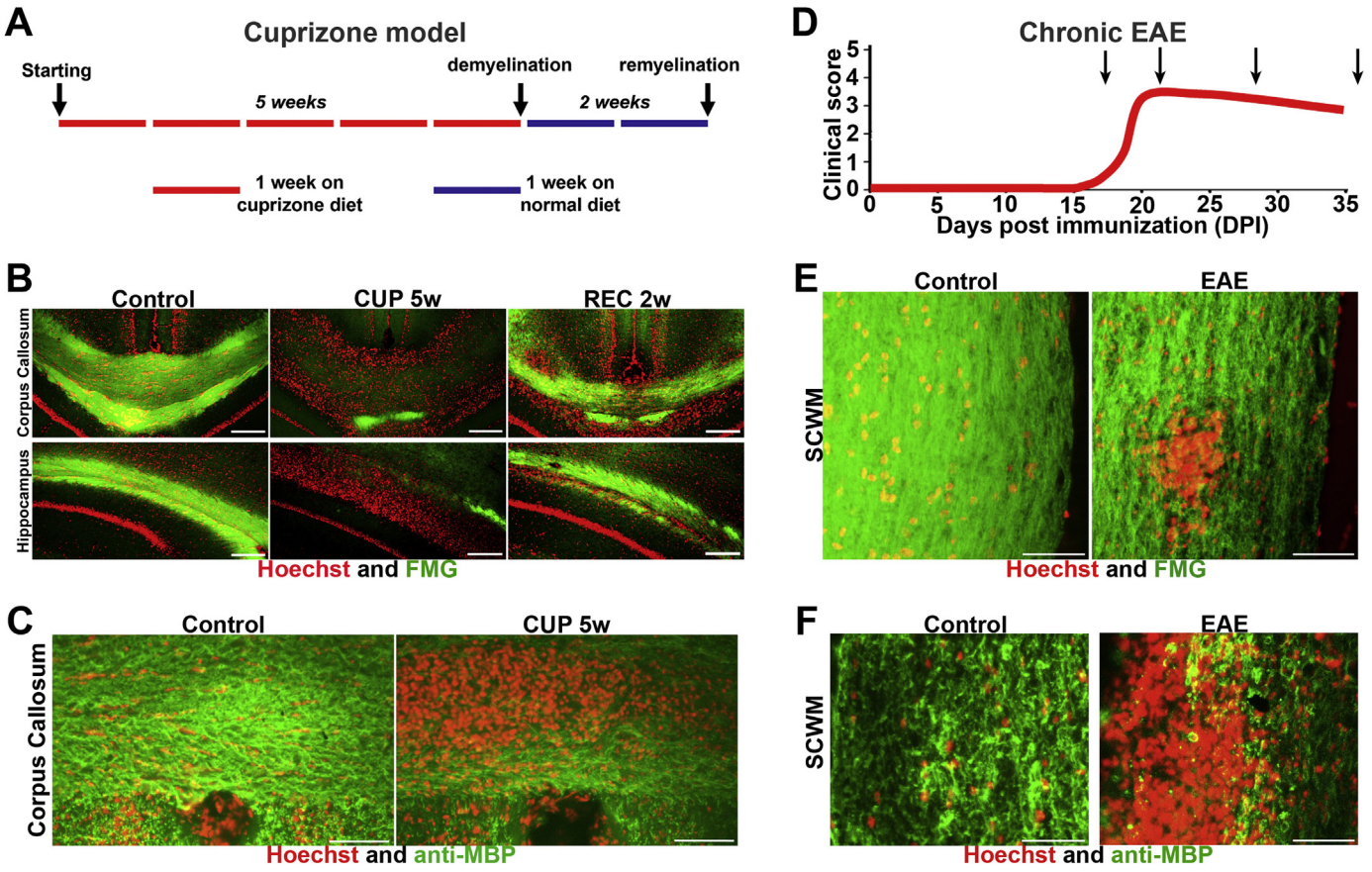

Fig. 1. Specific CNS demyelination in cuprizone and EAE models.
A, The experimental diagram of the cuprizone model. B, WM demyelination in corpus callosum (top) and the fimbria of hippocampus (bottom) of the cuprizone model is revealed by FluoroMyelin green (FMG, green) and the nuclear dye Hoechst (red) staining. C, Demyelination in corpus callosum revealed by Hoechst (red) staining and anti-MBP antibody (green) staining. D, A diagram of typical chronic EAE progression. Black arrows, 5 EAE mice used in the present study at different EAE stages. E, WM myelin (FMG in green) and EAE lesion (Hoechst in red) in the longitudinal sections of spinal cord of control (left) and EAE (right) mice. F, WM myelin (anti-MBP staining signals in green) and EAE lesion (Hoechst in red) in the longitudinal sections of spinal cord of control (left) and EAE (right) mice. Scale bars, 250 μm in B, and 50 μm in C–F. (For interpretation of the references to color in this figure legend, the reader is referred to the web version of this article.)

blocking solution. These were counterstained in nuclear dye (Hoechst 33342, purchased from Invitrogen, CA, USA) for 10 min, and again rinsed 5 × 5 min at RT. Slides were coverslipped using tris-buffered Fluoro-Gel mounting media (Electron Microscopy Sciences, PA, USA).

2.5. Conventional fluorescence microscopy and image quantification

Fluorescence microscopy and image analysis procedures were adapted from previously published methods (Jukkola et al., 2012; Jukkola et al., 2013; Jukkola et al., 2017). Images were captured using a Spot CCD camera RT slider (Diagnostic Instruments, Sterling Heights, MI, USA) in a Zeiss Axiophot upright microscope with 20 × 1Plan Apo objectives and saved as 16-bit TIFF files. Appropriate exposure times were used so the pixel intensities in the area of interest were below saturation, with the same exposure times used for each group within an experiment. Images for quantification were chosen from 8 representative experiments for MBP antibody, 2 for other antibodies, and compared between experimental cohorts (5 mice for each experimental cohort except cuprizone peak, 4). Images were analyzed with NIH ImageJ. MBP quantification was estimated using percent area after setting image-appropriate intensity thresholds, reflecting overall density of MBP expression. Staining intensities for GFAP were measured using the Image J tracing tool to trace and automatically calculate the average pixel fluorescence intensities of the outline drawn on astrocyte soma and processes (4–6 sampled per image). These intensities were averaged for each image, and the background intensity of the slide was subtracted for each image. The data was normalized to controls from the same staining experiments, as to account for variations in staining intensity. The image fluorescence intensity values were averaged to obtain the mean fluorescence intensity for each experimental group. These fluorescence intensity measurements reflect the level of protein present within the cells stained by a particular antibody (higher intensity correlates with more protein). All fluorescence intensity measurements were taken from the originally captured image. For representative images shown in the figures, image brightness and contrast were adjusted using Adobe Photoshop 7.0 (Adobe Systems Incorporated, CA, USA).

2.6. Confocal microscopy and 3D reconstruction

High-magnification confocal images were captured with a Leica TCS SL confocal imaging system (Leica Microsystems, Germany), using a 100× HCX Plan Apo CS oil immersion objective (numerical aperture = 1.00). Multiple channels were acquired simultaneously, and the signal was averaged over four scans. Channel crosstalk was largely eliminated through optimization of the laser line intensity by acousto-optical tunable excitation filters, and by spectral detectors allowing precisely-defined bandwidth adjustment. Images were saved as 8-bit TIFF files and adjusted for brightness and contrast using Adobe Photoshop 7.0. The procedure was described in details in our previous papers (Jukkola et al., 2012; Jukkola et al., 2013; Jukkola et al., 2017). The collapsed 2D image from each image stack is shown in the figures.

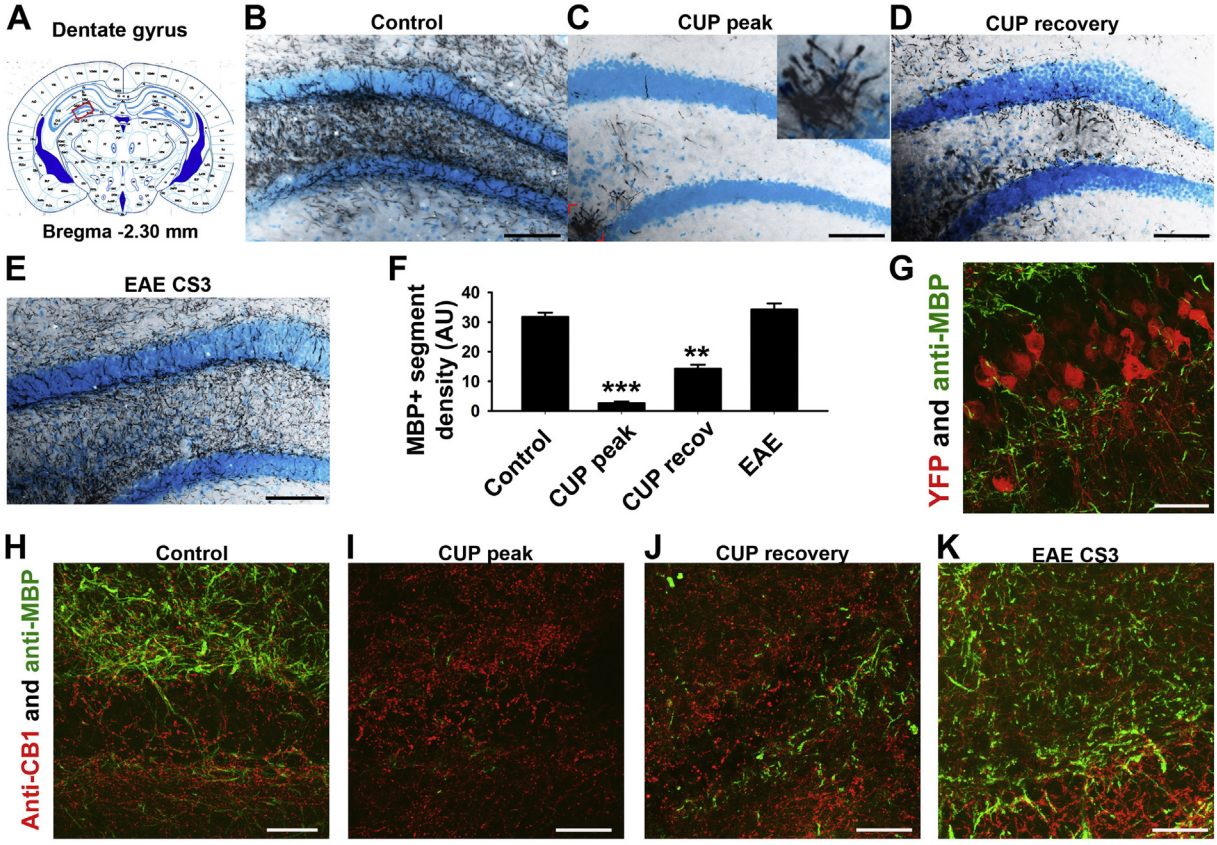

Fig. 2. Myelin alterations in dentate gyrus of the cuprizone and EAE mice.
A, Diagram map of dentate gyrus in the dorsal hippocampus of a coronal section of the brain. B, GM myelin in the DG of a control mouse (Control). C, GM myelin at the peak stage of cuprizone mouse (CUP peak). The insert, 3 fold higher magnification of cornered area showing myelin segments from a potential surviving oligodendrocyte. D, GM myelin at the recovery stage of cuprizone model (CUP recovery). E, GM myelin of an EAE mice with CS of 3 (EAE CS3). B-E, anti-MBP staining in black and Hoechst staining in blue. F, Summary of altered myelin density in DG. One way ANOVA followed by Dunnett's test: ***, $p < .001$; **, $p < .01$. n = 15 for every condition. G, Confocal image of GM myelin (anti-MBP in green) and dentate granule cells (YFP in red) from a control mice carrying Thy1-YFP transgene. H-K, Confocal images of DG regions with the staining for endogenous MBP (green) and CB1 (red) under the four different conditions. Scale bars, 250 μm in B-E and 50 μm in G-K. (For interpretation of the references to color in this figure legend, the reader is referred to the web version of this article.)

2.7. Statistical analysis

Statistical significance was determined using Sigmaplot 12.0 (Systat Software, Inc., IL, USA). One-way ANOVA followed by Dunnett's test was used for comparing experimental groups to one control group. *, $p < .05$ and **, $p < .01$ were considered statistically significant. Statistically significant differences from the control group are shown by an asterisk (*) in figures. Results are presented as means ± SEM.

3. Results

3.1. Demyelination of corpus callosum and spinal cord in the cuprizone and EAE mice, respectively

To validate the cuprizone and EAE mouse models used in the present study, their signature demyelination patterns in specific CNS regions were first examined. WM demyelination and remyelination of some brain regions in the cuprizone model was previously investigated. In particular, extensive demyelination of the corpus callosum has been well documented in the cuprizone model (Matsushima and Morell, 2001). Following five weeks of cuprizone ingestion, we found a marked reduction of myelin density in corpus callosum, shown by decreased Fluoromyelin Green (FMG) and myelin basic protein (MBP) levels (Fig. 1A–C). MBP is a reliable marker for mature myelin segments. After removing cuprizone from the diet for two weeks, myelin density clearly and partially recovered (Fig. 1A–C). Similar demyelination followed by remyelination in the cuprizone model was observed in the fimbria of hippocampus (Fig. 1B). In sharp contrast, these results of demyelination and remyelination were not seen following induction of EAE in corpus callosum, although demyelinated lesions were clearly present in spinal cord of the same EAE mice (Fig. 1D–F). These findings are consistent with our previous results (Jukkola et al., 2012; Jukkola et al., 2013; Jukkola et al., 2017). These lesions in spinal cord contribute to clinical signs observed in these EAE mice. In the present study, we used five mice with clinical scores ranging from 3 to 4 and at various days post immunization (DPI), with one mouse each at DPI17, DPI21 and DPI28, and two mice at DPI72. Every one of these EAE mice showed extensive lesions throughout the spinal cord, labeled with FMG and MBP staining. By contrast, no such lesion was observed in spinal cord of the cuprizone model. Therefore, myelination is differentially affected by the two models in different CNS regions.

3.2. Reduction of gray matter myelination in hippocampal dentate gyrus in the cuprizone but not EAE mice

To determine how myelination in the hippocampal-prefrontal pathway is altered in the two mouse models, we first focused on potential myelin alterations in the hippocampus. The entorhinal cortex feeds signals from cortical and subcortical structures to the hippocampus via the perforant path, starting the trisynaptic neural circuit. The flow of information in the hippocampus is believed to be largely unidirectional. Axons in the perforant path mainly project to the

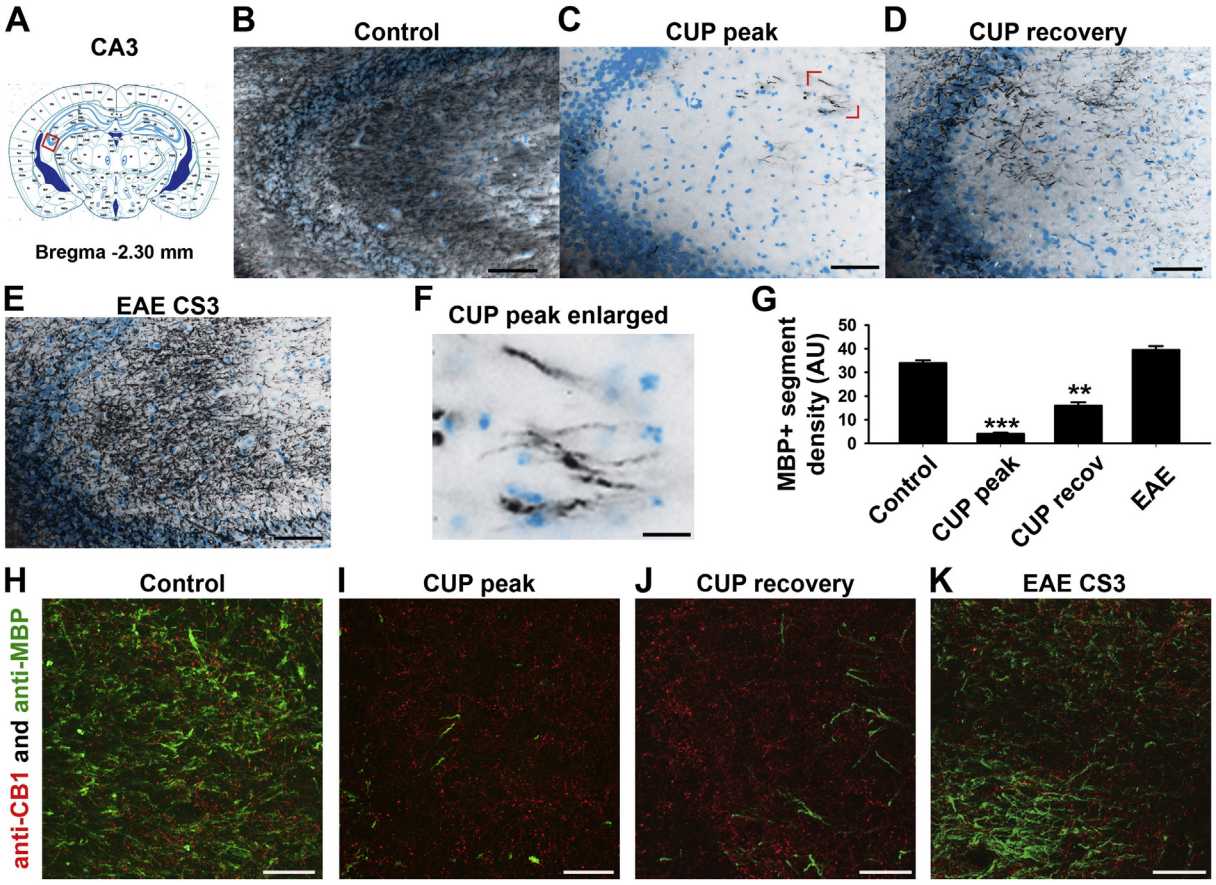

Fig. 3. Myelin alterations in the CA3 region of the cuprizone and EAE mice.
A, Diagram map of the CA3 region of a coronal section of the brain. B, GM myelin in the CA3 region of a control mouse (Control). C, GM myelin at the peak stage of cuprizone mouse (CUP peak). D, GM myelin at the recovery stage of cuprizone model (CUP recovery). E, GM myelin of an EAE mice with CS of 3 (EAE CS3). B-E, anti-MBP staining in black and Hoechst staining in blue. F, An enlarged image (3 fold higher magnification) of the cornered area in C, showing myelin segments from a potential surviving oligodendrocyte. G, Summary of altered myelin density in CA3. One way ANOVA followed by Dunnett's test: ***, $p < .001$; **, $p < .01$. n = 17 for every condition. H-K, Confocal images of CA3 regions with the staining for endogenous MBP (green) and CB1 (red) under the four different conditions. Scale bars, 250 μm in B-E and 50 μm in F,H-K. (For interpretation of the references to color in this figure legend, the reader is referred to the web version of this article.)

granule cells in the dentate gyrus (DG), and the DG axons pass on the information to the dendrites of CA3 pyramidal cells, which then extend to CA1. Axons from CA1 then project back to the entorhinal cortex, or extend to other cortical areas, such as the PFC. We stained the sections of brains from control, cuprizone or EAE mice for MBP and examined the distribution pattern of myelin segments in different hippocampal subregions, focusing on gray matter (GM).

The DG is a part of GM regions in the brain (Fig. 2A), but clearly contains myelin in both granular and polymorph DG. Normally, myelin segments were organized throughout the granule cell layer, and relatively denser with multiple dimensions throughout the hilus (Fig. 2B). Five weeks of cuprizone ingestion led to significant reduction in the density of MBP-positive myelin segments throughout the DG, sometimes with a few individual myelin segments and/or patches of segments present in the hilus (Fig. 2C). These patches resembled the individual mature oligodendrocytes with multiple myelin segments frequently observed in the myelin coculture (Gardner et al., 2012; Gu and Gu, 2011), and thus likely represented surviving oligodendrocytes (Fig. 2C). Two weeks after returning to normal chow, the cuprizone-fed mice regained some myelin segments throughout the hilus and granule cell layer, although still significantly less than control in density (Fig. 2D). Recovered myelin segments also appeared shorter than those in the control. In sharp contrast, there was no clear reduction of the density of MBP-positive myelin segments in the DG of EAE mice (Fig. 2B–F), with similar MBP patterns as control. To visualize the relative location between myelin segments and DG neurons, we performed confocal imaging on brain sections from Thy1-YFP transgenic mice. MBP+ myelin segments were close but not colocalize with YFP-positive DG neuron soma and dendrites (Fig. 2G).

To further examine the localization of myelin segments with axons in DG, we performed confocal imaging for endogenous MBP and cannabinoid receptor type 1 (CB1) (Fig. 2H–K). Cannabinoids may be developed to treat MS patients. It was reported that a potent CB1 agonist WIN55, 212-2, effectively delayed disease progression in EAE mice (de Lago et al., 2012), while CB1 knockout mice showed a more severe EAE clinical course (Rossi et al., 2011). CB1 is a G protein-coupled receptor protein present in preterminal/terminal axons, and are abundant in GABAergic interneurons of the hippocampus (Lou et al., 2012; Miller and Devi, 2011). We found that there was no colocalization between MBP and CB1 in the DG of control, cuprizone and EAE mice (Fig. 2H–K). Whereas MBP density was greatly diminished at cuprizone peak, there was no clear change in CB1 expression and density (Fig. 2I). Thus, CB1 seems mainly present in unmyelinated axons.

3.3. Differential alterations of myelin density in hippocampal CA3/CA1 regions between the two MS models

Axons from the DG granule neurons mainly target the dendrites of pyramidal cells in CA3 to form synapses in the hippocampus. Normal myelination of the axons transmitting these inputs in CA3 shows an organized pattern throughout the pyramidal cell layer, and more dense and unorganized throughout the molecular layer (Fig. 3A,B). Similar to

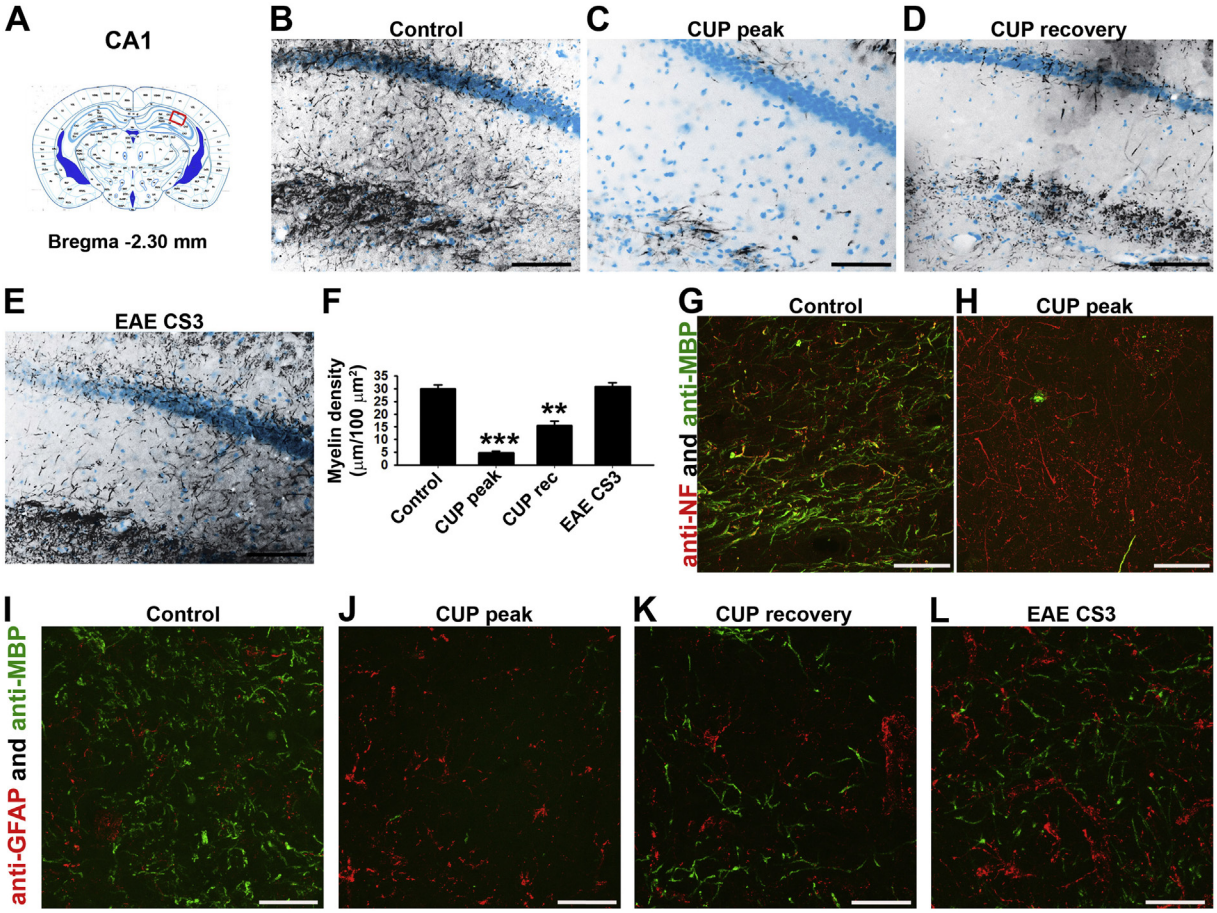

Fig. 4. Myelin alterations in the CA1 region of the cuprizone and EAE mice.
A, Diagram map of the CA1 region in a coronal section of the brain. B, GM myelin in the CA1 region of a control mouse (Control). C, GM myelin at the peak stage of cuprizone mouse (CUP peak). D, GM myelin at the recovery stage of cuprizone model (CUP recovery). E, GM myelin of an EAE mice with CS of 3 (EAE CS3). B-E, anti-MBP staining in black and Hoechst staining in blue. F, Summary of altered myelin density in CA1. One way ANOVA followed by Dunnett's test: ***, $p < .001$; **, $p < .01$. n = 15 for every condition. G,H, Confocal images for endogenous MBP (green) and NF (red) in CA1. I-L, Confocal images of CA1 regions with the staining for endogenous MBP (green) and GFAP (red) under the four different conditions. Scale bars, 250 μm in B-E and 50 μm in G-L. (For interpretation of the references to color in this figure legend, the reader is referred to the web version of this article.)

the DG, the CA3 region showed extensive decrease in MBP+ myelin density at the cuprizone peak stage, less reduction at the recovery stage, and no change in EAE model (Fig. 3B–G). Throughout the pyramidal cell layer at the peak cuprizone stage, almost no MBP expression remained, and only small patches, resembling individual oligodendrocytes, of MBP+ segments throughout the molecular level remained (Fig. 3F). At the recovery stage, the CA3 partially regained MBP density in the cell layer, and in patches throughout the molecular level. The MBP+ segments were significantly shorter than control. High resolution confocal images revealed the changes of myelin densities at the peak and recovery stages of the cuprizone model, as well as no significant change of myelin density in EAE (Fig. 3H–K). CB1 expression was high in the CA3 region, but had no colocalization with MBP and no clear change in cuprizone and EAE models (Fig. 3H–K).

CA3 pyramidal neurons send their axons to the dendrites of CA1 pyramidal neurons, while the CA1 axons exit the hippocampus to project to other CNS regions, including PFC. The pattern of myelin segments in CA1 was similar to that in CA3, albeit being less dense in the molecular level (Fig. 4A,B). At cuprizone peak, almost all MBP+ myelin segments disappeared in both the cell layer and molecular layer (Fig. 4C). The remaining ones were in patches, similar to those seen in the other hippocampal regions. At the recovery stage, MBP+ myelin segments appeared in both the cell body layer and molecular level, although segments were shorter with more anterior-to-posterior orientation (Fig. 4D). Again, we failed to observe any changes in terms of MBP+ myelin density and MBP signal intensity (Fig. 4E,F). To determine whether the reduction of MBP+ myelin density was due to loss of myelin or axons, we double-stained for MBP and neurofilament (NF), an intermediate filament highly expressed in neurons. Within all regions of the hippocampus and under various experimental conditions, there was no clear change in NF levels and NF+ axonal density. In the CA1 region, MBP and NF were highly colocalized under control condition, whereas MBP+ myelin segments but not NF+ axonal density markedly decreased at the peak stage of the cuprizone model (Fig. 4G,H).

To examine alterations of astrocytes in cuprizone and EAE models, we co-stained brain sections for MBP and glial fabrillary acidic protein (GFAP), an intermediate filament mainly expressed in astrocytes. In the CA1 region, MBP and GFAP staining signals did not colocalize under the control condition (Fig. 4I). GFAP expression significantly increased at the peak and recovery stages of the cuprizone model, as well as in the EAE model (Fig. 4I–L). This is different from alterations of MBP+ myelin density under these conditions (Fig. 4B–L). These findings are consistent with our previous results showing increased GFAP expression in the hippocampus of the EAE model (Jukkola et al., 2013), and another study using the cuprizone model (Koutsoudaki et al., 2009).

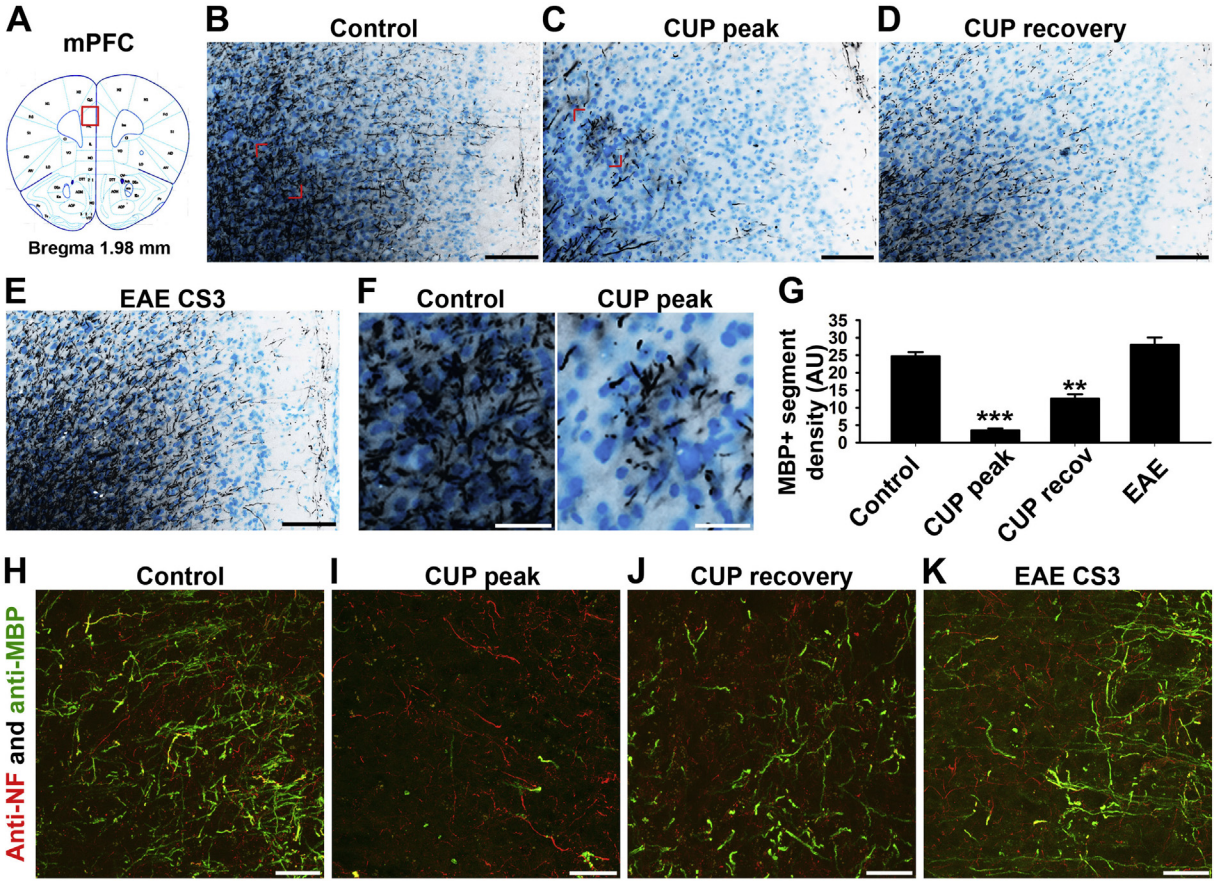

Fig. 5. Myelin alterations in mPFC of the cuprizone and EAE mice.
A, Diagram map of the mPFC of a coronal section of the brain. B, GM myelin in mPFC of a control mouse (Control). C, GM myelin at the peak stage of cuprizone mouse (CUP peak). D, GM myelin at the recovery stage of cuprizone model (CUP recovery). E, GM myelin of an EAE mice with CS of 3 (EAE CS3). F, Enlarged images of cornered areas in B (left) and C (right). B-F, anti-MBP staining in black and Hoechst staining in blue. G, Summary of altered myelin density in mPFC. One way ANOVA followed by Dunnett's test: ***, $p < .001$; **, $p < .01$. n = 14 for every condition. H-K, Confocal images of mPFC regions with the staining for endogenous MBP (green) and NF (red) under the four different conditions. Scale bars, 250 μm in B-E and 50 μm in F,H-K. (For interpretation of the references to color in this figure legend, the reader is referred to the web version of this article.)

3.4. Alterations of gray matter myelination in the PFC in cuprizone and EAE mice

An important projection facilitating memory encoding and subsequent retrieval involves the interplay of the hippocampus and a region of the PFC, the medial PFC (mPFC). This interaction plays a key role in working memory, episodic memory and emotional memory via direct and indirect paths, allowing for behaviors modulated by past experiences. Normal myelinated axons of the mPFC, responsible for facilitating this interaction, extend laterally from the midline in an organized fashion (Fig. 5A,B). MBP+ myelin density markedly reduced at the peak and recovery stages of the cuprizone model, but remained unchanged in the EAE model (Fig. 5B–G). Isolated clusters of MBP+ myelin segments were observed at the peak stage of cuprizone model (Fig. 5F), likely representing surviving mature oligodendrocytes. Confocal imaging of NF and MBP costaining further confirmed that GM myelin reduction resulted from demyelination but not axon degradation in the cuprizone model (Fig. 5H–J). Interestingly, we did not observe any clear reduction of MBP+ myelin density in the EAE model (Fig. 5K).

The axons from CA1 pyramidal neurons also project to the lateral region of the PFC, agranular insular dorsal cortex (AID) (Fig. 6A) (Cenquizca and Swanson, 2007). AID plays a key role in object recognition memory and extinction learning (Bermudez-Rattoni et al., 2005), and regulates the cued reinstatement of drug-seeking, but not food-seeking, behavior in rats (Contreras et al., 2012; Cosme et al., 2015). Typical GM myelination with mesh-like network of MBP+ myelin segments was observed in AID (Fig. 6B). Myelin density markedly reduced at the peak and recovery stages of the cuprizone model, but remained unchanged in the EAE model (Fig. 6B–F). In Thy1-YFP transgenic mice, pyramidal neuron dendrites with abundant dendritic spines were present in AID, where MBP+ myelin segments were present (Fig. 6G). Reduction of myelin density in the cuprizone model was due to loss of myelin, rather than axonal loss, revealed by confocal imaging for MBP and NF co-staining (Fig. 6H). These patches are similar to those found in the hippocampus. Removal of cuprizone allowed for partial recovery of myelin density throughout all layers of the cortex, but the segments were noticeably shorter than myelin segments in control. Again, there was no clear change in MBP+ myelin density in EAE mice (Fig. 6E–H).

4. Discussion

The present study showed that myelin density in the hippocampus and PFC was differentially altered in the two established mouse models of MS, the cuprizone and chronic EAE models. After 5 weeks of cuprizone intake, GM myelin density markedly decreased in various subregions of the hippocampus and PFC. After 2 weeks of returning to normal diet, myelin density clearly and partially recovered in these regions. In sharp contrast, there was no significant reduction of myelin density in these regions at both peak and late stages of EAE mice. Taken together, cuprizone toxicity and autoimmunity differentially impact

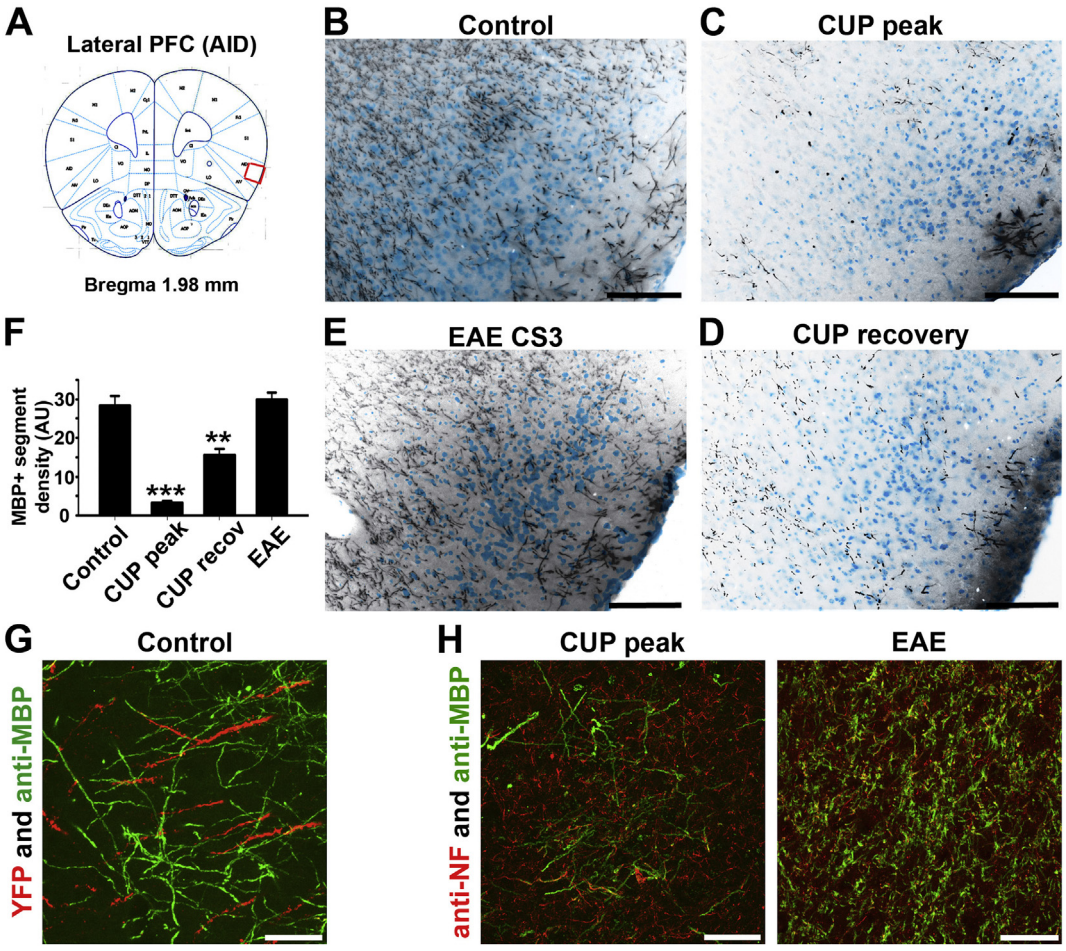

Fig. 6. Myelin alterations in agranular insular cortex of the cuprizone and EAE mice.
A, Diagram map of agranular insular cortex of a coronal section of the brain. B, GM myelin in agranular insular cortex (AID) of a control mouse (Control). C, GM myelin at the peak stage of cuprizone mouse (CUP peak). D, GM myelin at the recovery stage of cuprizone model (CUP recovery). E, GM myelin of an EAE mice with CS of 3 (EAE CS3). B-E, anti-MBP staining in black and Hoechst staining in blue. F, Summary of altered myelin density in AID. One way ANOVA followed by Dunnett's test: ***, $p < .001$; **, $p < .01$. n = 13 for every condition. G, Confocal image of myelin (anti-MBP in green) and pyramidal neuron dendrites (YFP in red) from a control mice carrying Thy1-YFP transgene. H, Confocal image with the staining for endogenous MBP (green) and NF (red) at the peak stage of the cuprizone model (CUP peak) and at the peak stage of EAE (EAE). Scale bars, 250 μm in B-E and 50 μm in G-H. (For interpretation of the references to color in this figure legend, the reader is referred to the web version of this article.)

myelin density in GM of the brain, mimicking different aspects of demyelinating diseases.

Throughout our studies, we found significant and consistent reduction of myelin density induced by cuprizone intake in not only typical WM of the brain including corpus callosum (Fig. 1), but also GM including the hippocampus and PFC (Figs. 2–6). Our results are consistent with earlier studies reporting widespread demyelination of the brain in the cuprizone model (Dutta et al., 2013; Gudi et al., 2009; Kipp et al., 2017). Mature myelin segments in WM and GM reside in different microenvironments. For instance, GM myelin is often located adjacent to neuronal cell bodies, dendrites and synapses, whereas WM myelin is not. Thus, GM and WM myelination may be regulated differently. Our studies showed that myelin density in both WM and GM including corpus callosum, hippocampus and PFC, reduced at the peak stage of the cuprizone model, which does not exclude potential quantitative differences across various brain regions. While we were examining GM myelin density in the cuprizone model, we often observed isolated clusters of myelin segments at the peak stage and sometimes the recovery stage as well (Figs. 2C, 3F, 5F). These clusters of myelin segments resemble the morphology of multiple MBP+ myelin segments of a mature oligodendrocyte (Gardner et al., 2012; Gu and Gu, 2011). Whether these patches are surviving oligodendrocytes during massive demyelination or newly differentiated oligodendrocytes for remyelination remain to be determined in future studies. Recent studies reported that GM myelin segments in layers 2 and 3 of neocortex (~50%) and in the hippocampus (~80%) ensheath the axons from parvalbumin-positive GABAergic interneurons (Micheva et al., 2016; Stedehouder et al., 2017). Therefore, it will be interesting to determine which type of axons (e.g. glutamatergic versus GABAergic) is demyelinated or remyelinated first in a specific brain region at different stages of the cuprizone model.

Our recent studies showed EAE lesions containing demyelination in spinal cord and cerebellum (Jukkola et al., 2017), and altered astrocytes in various brain regions of EAE mice (Jukkola et al., 2013). However, we failed to observe any significant reduction of GM myelin density in the hippocampus and PFC of EAE mice (Figs. 2–6), as well as other several brain regions. This is in stark contrast with several earlier studies showing demyelination in the hippocampus and cortex (Aharoni et al., 2019; Girolamo et al., 2011; Sun et al., 2015; Ziehn et al., 2010). Interestingly, one recent study reported that there were significant decreases in both MBP and synaptophysin (a presynaptic marker) immunoreactivity at DPI14 and DPI35, but not in the control nor at DPI21 and DPI100 (Burns et al., 2014). Our EAE samples were obtained from mice with early to late EAE, and consistently showed no significant

change in myelin density. Importantly, in these EAE mice used in our study, the spinal cord and the brain were sectioned onto the same slide. We routinely verified EAE lesions in spinal cord while we were examining myelin density in the brain. Currently, it is not clear what caused such differences. At the same time, we cannot exclude possible alterations of myelin membranes in EAE brains at the ultrastructural level.

Using NF as an axonal marker, we found that MBP+ myelin segments formed along NF+ axons and there was no clear reduction of NF + axonal density in the cuprizone and EAE models (Figs. 4G,H, 5G–K, 6H). CB1 is another axonal marker we examined in this study. Cannabinoids carry out their functions mainly through two receptors, CB1 and CB2, although additional receptors are implicated (Pertwee et al., 2010). CB1s are mainly expressed in the CNS and distributed in axonal terminals (Lou et al., 2012; Miller and Devi, 2011), whereas CB2s are mainly expressed in immune cells (Atwood and Mackie, 2010; Klein et al., 2003). Our results showed that there was no colocalization between MBP and CB1 in the hippocampus of control, cuprizone and EAE mice (Figs. 2, 3), consistent with the localization pattern of CB1 in axonal terminals and presynaptic sites, which are not myelinated. Therefore, our findings do not argue against a potential regulatory role of cannabinoid pathways in myelination or multiple sclerosis.

The autoimmune response in EAE is mainly mediated by MHC Class II restricted CD4+ T-lymphocytes (Lassmann and Bradl, 2017). Immune cells that infiltrate into the CNS can be easily observed in spinal cord and the cerebellum (Jukkola et al., 2012; Jukkola et al., 2017). In the hippocampus and cortex of EAE mice, localized presence of ramified and hypertrophied microglia/macrophages (CD45+ or Iba1), T cells (CD3) and B cells (CD19) was also observed (Kocovski et al., 2019; Mangiardi et al., 2011). In contrast, the cuprizone model involves apoptosis of oligodendrocytes, demyelination and activated microglia, but not infiltrating immune cells (Lassmann and Bradl, 2017; Ransohoff, 2012).

Astrocytes were viewed as cells that promote inflammation and form glial scars that hinder remyelination and axon growth in the past. We now know that astrocytes can enhance CNS myelination by promoting the migration, proliferation, and differentiation of oligodendrocyte progenitor cells (Ishibashi et al., 2006; Nash et al., 2011; Watkins et al., 2008). Our results showed that GFAP expression was significantly upregulated in the hippocampus at the peak and recovery stages of the cuprizone model, as well as in the EAE model (Fig. 4I–L). This is consistent with our previous findings in the EAE mice (Jukkola et al., 2013). Although GFAP expression was significantly upregulated, myelin density in the hippocampus remained unchanged in the EAE mice but markedly reduced in the cuprizone model (Figs. 2–4). Thus, astrocyte activation may not always correlate with myelination or demyelination in the brain.

While the chronic EAE is a well-established model for studying the autoimmune aspect of MS, our study showed that the cuprizone model may be better suited for investigating the role of demyelination in hippocampal-prefrontal circuit in MS-related cognitive deficits. More research is needed to fully understand the impact of myelination of the hippocampal-prefrontal circuit on cognitive functions. To further elucidate molecular mechanisms underlying GM myelin may uncover new targets for therapy of various demyelinating diseases. Taken together, although the cuprizone model's mode of demyelination is not similar to most MS lesions, the model provides results that align with MS demyelination patterns and physiology, and should be further studied to discern myelin's role in cognitive impairment.

Author contributions

C.G. designed and supervised the research. M.N., F.E., and P.J. performed experiments and analyzed data. M.N. made figures and wrote the first draft of the manuscript. C.G. revised figures and the manuscript. All the authors participated in revising the manuscript.

Declaration of Competing Interest

The authors declare no competing interests.

Acknowledgement

We thank James Rice and Davin Packer for technical assistance. This work was supported in part by grants from NIH (R01NS093073 and R21AA024873) to CG.

References

Abraham, H., Vincze, A., Jewgenow, I., Veszpremi, B., Kravjak, A., Gomori, E., Seress, L., 2010. Myelination in the human hippocampal formation from midgestation to adulthood. Int. J. Dev. Neurosci. 28, 401–410.
Achiron, A., Barak, Y., 2003. Cognitive impairment in probable multiple sclerosis. J. Neurol. Neurosurg. Psychiatry 74, 443–446.
Aharoni, R., Schottlender, N., Bar-Lev, D.D., Eilam, R., Sela, M., Tsoory, M., Arnon, R., 2019. Cognitive impairment in an animal model of multiple sclerosis and its amelioration by glatiramer acetate. Sci. Rep. 9, 4140.
Atwood, B.K., Mackie, K., 2010. CB2: a cannabinoid receptor with an identity crisis. Br. J. Pharmacol. 160, 467–479.
Baecher-Allan, C., Kaskow, B.J., Weiner, H.L., 2018. Multiple sclerosis: mechanisms and immunotherapy. Neuron 97, 742–768.
Barry, J., Gu, Y., Jukkola, P., O'Neill, B., Gu, H., Mohler, P.J., Rajamani, K.T., Gu, C., 2014. Ankyrin-G directly binds to Kinesin-1 to transport voltage-gated Na^+ channels into axons. Dev. Cell 28, 117–131.
Bartzokis, G., Lu, P.H., Mintz, J., 2007. Human brain myelination and amyloid beta deposition in Alzheimer's disease. Alzheimers Dement. 3, 122–125.
Bermudez-Rattoni, F., Okuda, S., Roozendaal, B., McGaugh, J.L., 2005. Insular cortex is involved in consolidation of object recognition memory. Learn. Mem. 12, 447–449.
Burns, T., Miers, L., Xu, J., Man, A., Moreno, M., Pleasure, D., Bannerman, P., 2014. Neuronopathy in the motor neocortex in a chronic model of multiple sclerosis. J. Neuropathol. Exp. Neurol. 73, 335–344.
Cenquizca, L.A., Swanson, L.W., 2007. Spatial organization of direct hippocampal field CA1 axonal projections to the rest of the cerebral cortex. Brain Res. Rev. 56, 1–26.
Contreras, M., Billeke, P., Vicencio, S., Madrid, C., Perdomo, G., Gonzalez, M., Torrealba, F., 2012. A role for the insular cortex in long-term memory for context-evoked drug craving in rats. Neuropsychopharmacology 37, 2101–2108.
Cosme, C.V., Gutman, A.L., LaLumiere, R.T., 2015. The dorsal agranular insular cortex regulates the cued reinstatement of cocaine-seeking, but not food-seeking, behavior in rats. Neuropsychopharmacology 40, 2425–2433.
de Lago, E., Moreno-Martet, M., Cabranes, A., Ramos, J.A., Fernandez-Ruiz, J., 2012. Cannabinoids ameliorate disease progression in a model of multiple sclerosis in mice, acting preferentially through CB1 receptor-mediated anti-inflammatory effects. Neuropharmacology 62, 2299–2308.
Dutta, R., Chomyk, A.M., Chang, A., Ribaudo, M.V., Deckard, S.A., Doud, M.K., Edberg, D.D., Bai, B., Li, M., Baranzini, S.E., et al., 2013. Hippocampal demyelination and memory dysfunction are associated with increased levels of the neuronal microRNA miR-124 and reduced AMPA receptors. Ann. Neurol. 73, 637–645.
Eluvathingal, T.J., Chugani, H.T., Behen, M.E., Juhasz, C., Muzik, O., Maqbool, M., Chugani, D.C., Makki, M., 2006. Abnormal brain connectivity in children after early severe socioemotional deprivation: a diffusion tensor imaging study. Pediatrics 117, 2093–2100.
Flynn, S.W., Lang, D.J., Mackay, A.L., Goghari, V., Vavasour, I.M., Whittall, K.P., Smith, G.N., Arango, V., Mann, J.J., Dwork, A.J., et al., 2003. Abnormalities of myelination in schizophrenia detected in vivo with MRI, and post-mortem with analysis of oligodendrocyte proteins. Mol. Psychiatry 8, 811–820.
Franco-Pons, N., Torrente, M., Colomina, M.T., Vilella, E., 2007. Behavioral deficits in the cuprizone-induced murine model of demyelination/remyelination. Toxicol. Lett. 169, 205–213.
Frankland, P.W., Bontempi, B., 2005. The organization of recent and remote memories. Nat. Rev. 6, 119–130.
Gardner, A., Jukkola, P., Gu, C., 2012. Myelination of rodent hippocampal neurons in culture. Nat. Protoc. 7, 1774–1782.
Gaudino, E.A., Chiaravalloti, N.D., DeLuca, J., Diamond, B.J., 2001. A comparison of memory performance in relapsing-remitting, primary progressive and secondary progressive, multiple sclerosis. Neuropsychiatry Neuropsychol. Behav. Neurol. 14, 32–44.
Geurts, J.J., Bo, L., Roosendaal, S.D., Hazes, T., Daniels, R., Barkhof, F., Witter, M.P., Huitinga, I., van der Valk, P., 2007. Extensive hippocampal demyelination in multiple sclerosis. J. Neuropathol. Exp. Neurol. 66, 819–827.
Girolamo, F., Ferrara, G., Strippoli, M., Rizzi, M., Errede, M., Trojano, M., Perris, R., Roncali, L., Svelto, M., Mennini, T., et al., 2011. Cerebral cortex demyelination and oligodendrocyte precursor response to experimental autoimmune encephalomyelitis. Neurobiol. Dis. 43, 678–689.
Gu, C., Gu, Y., 2011. Clustering and activity tuning of kv1 channels in myelinated hippocampal axons. J. Biol. Chem. 286, 25835–25847.
Gu, Y., Jukkola, P., Wang, Q., Esparza, T., Zhao, Y., Brody, D., Gu, C., 2017. Polarity of varicosity initiation in central neuron mechanosensation. J. Cell Biol. 216, 2179–2199.
Gudi, V., Moharregh-Khiabani, D., Skripuletz, T., Koutsoudaki, P.N., Kotsiari, A., Skuljec,

J., Trebst, C., Stangel, M., 2009. Regional differences between grey and white matter in cuprizone induced demyelination. Brain Res. 1283, 127–138.
Haroutunian, V., Katsel, P., Roussos, P., Davis, K.L., Altshuler, L.L., Bartzokis, G., 2014. Myelination, oligodendrocytes, and serious mental illness. Glia 62, 1856–1877.
Ishibashi, T., Dakin, K.A., Stevens, B., Lee, P.R., Kozlov, S.V., Stewart, C.L., Fields, R.D., 2006. Astrocytes promote myelination in response to electrical impulses. Neuron 49, 823–832.
Jones, M.V., Nguyen, T.T., Deboy, C.A., Griffin, J.W., Whartenby, K.A., Kerr, D.A., Calabresi, P.A., 2008. Behavioral and pathological outcomes in MOG 35-55 experimental autoimmune encephalomyelitis. J. Neuroimmunol. 199, 83–93.
Jongen, P.J., Ter Horst, A.T., Brands, A.M., 2012. Cognitive impairment in multiple sclerosis. Minerva Med. 103, 73–96.
Jukkola, P.I., Lovett-Racke, A.E., Zamvil, S.S., Gu, C., 2012. K+ channel alterations in the progression of experimental autoimmune encephalomyelitis. Neurobiol. Dis. 47, 280–293.
Jukkola, P., Gray, V., Guerrero, T., Gu, C., 2013. Astrocytes differentially respond to inflammatory autoimmune insults and imbalances of neural activity. Acta Neuropathol. Commun. 1, 70.
Jukkola, P., Gu, Y., Lovett-Racke, A.E., Gu, C., 2017. Suppression of inflammatory demyelinaton and axon degeneration through inhibiting Kv3 channels. Front. Mol. Neurosci. 10, 344.
Kipp, M., Nyamoya, S., Hochstrasser, T., Amor, S., 2017. Multiple sclerosis animal models: a clinical and histopathological perspective. Brain Pathol. 27, 123–137.
Kitamura, T., Ogawa, S.K., Roy, D.S., Okuyama, T., Morrissey, M.D., Smith, L.M., Redondo, R.L., Tonegawa, S., 2017. Engrams and circuits crucial for systems consolidation of a memory. Science 356, 73–78.
Klein, T.W., Newton, C., Larsen, K., Lu, L., Perkins, I., Nong, L., Friedman, H., 2003. The cannabinoid system and immune modulation. J. Leukoc. Biol. 74, 486–496.
Kocovski, P., Jiang, X., D'Souza, C.S., Li, Z., Dang, P.T., Wang, X., Chen, W., Peter, K., Hale, M.W., Orian, J.M., 2019. Platelet depletion is effective in ameliorating anxiety-like behavior and reducing the pro-inflammatory environment in the hippocampus in murine experimental autoimmune encephalomyelitis. J. Clin. Med. 8.
Koutsoudaki, P.N., Skripuletz, T., Gudi, V., Moharregh-Khiabani, D., Hildebrandt, H., Trebst, C., Stangel, M., 2009. Demyelination of the hippocampus is prominent in the cuprizone model. Neurosci. Lett. 451, 83–88.
Lassmann, H., Bradl, M., 2017. Multiple sclerosis: experimental models and reality. Acta Neuropathol. 133, 223–244.
Li, L., Lei, D., Li, L., Huang, X., Suo, X., Xiao, F., Kuang, W., Li, J., Bi, F., Lui, S., et al., 2016. White matter abnormalities in post-traumatic stress disorder following a specific traumatic event. EBioMedicine 4, 176–183.
Liu, J., Dietz, K., DeLoyht, J.M., Pedre, X., Kelkar, D., Kaur, J., Vialou, V., Lobo, M.K., Dietz, D.M., Nestler, E.J., et al., 2012. Impaired adult myelination in the prefrontal cortex of socially isolated mice. Nat. Neurosci. 15, 1621–1623.
Lou, Z.Y., Zhao, C.B., Xiao, B.G., 2012. Immunoregulation of experimental autoimmune encephalomyelitis by the selective CB1 receptor antagonist. J. Neurosci. Res. 90, 84–95.
Makinodan, M., Rosen, K.M., Ito, S., Corfas, G., 2012. A critical period for social experience-dependent oligodendrocyte maturation and myelination. Science 337, 1357–1360.
Mangiardi, M., Crawford, D.K., Xia, X., Du, S., Simon-Freeman, R., Voskuhl, R.R., Tiwari-Woodruff, S.K., 2011. An animal model of cortical and callosal pathology in multiple sclerosis. Brain Pathol. 21, 263–278.
Matsushima, G.K., Morell, P., 2001. The neurotoxicant, cuprizone, as a model to study demyelination and remyelination in the central nervous system. Brain Pathol. 11, 107–116.
Micheva, K.D., Wolman, D., Mensh, B.D., Pax, E., Buchanan, J., Smith, S.J., Bock, D.D., 2016. A large fraction of neocortical myelin ensheathes axons of local inhibitory neurons. eLife 5.
Miller, L.K., Devi, L.A., 2011. The highs and lows of cannabinoid receptor expression in disease: mechanisms and their therapeutic implications. Pharmacol. Rev. 63, 461–470.
Miller, D.J., Duka, T., Stimpson, C.D., Schapiro, S.J., Baze, W.B., McArthur, M.J., Fobbs, A.J., Sousa, A.M., Sestan, N., Wildman, D.E., et al., 2012. Prolonged myelination in human neocortical evolution. Proc. Natl. Acad. Sci. U. S. A. 109, 16480–16485.
Nash, B., Thomson, C.E., Linington, C., Arthur, A.T., McClure, J.D., McBride, M.W., Barnett, S.C., 2011. Functional duality of astrocytes in myelination. J. Neurosci. 31, 13028–13038.
Nickel, M., Gu, C., 2018. Regulation of central nervous system myelination in higher brain functions. Neural Plast. 2018, 6436453.
Olsson, T., Barcellos, L.F., Alfredsson, L., 2017. Interactions between genetic, lifestyle and environmental risk factors for multiple sclerosis. Nat. Rev. Neurol. 13, 25–36.
Pertwee, R.G., Howlett, A.C., Abood, M.E., Alexander, S.P., Di Marzo, V., Elphick, M.R., Greasley, P.J., Hansen, H.S., Kunos, G., Mackie, K., et al., 2010. International Union of Basic and Clinical Pharmacology. LXXIX. Cannabinoid receptors and their ligands: beyond CB(1) and CB(2). Pharmacol. Rev. 62, 588–631.
Peruga, I., Hartwig, S., Thone, J., Hovemann, B., Gold, R., Juckel, G., Linker, R.A., 2011. Inflammation modulates anxiety in an animal model of multiple sclerosis. Behav. Brain Res. 220, 20–29.
Pollak, Y., Orion, E., Goshen, I., Ovadia, H., Yirmiya, R., 2002. Experimental autoimmune encephalomyelitis-associated behavioral syndrome as a model of 'depression due to multiple sclerosis. Brain Behav. Immun. 16, 533–543.
Rajkowska, G., Mahajan, G., Maciag, D., Sathyanesan, M., Iyo, A.H., Moulana, M., Kyle, P.B., Woolverton, W.L., Miguel-Hidalgo, J.J., Stockmeier, C.A., et al., 2015. Oligodendrocyte morphometry and expression of myelin - related mRNA in ventral prefrontal white matter in major depressive disorder. J. Psychiatr. Res. 65, 53–62.
Ransohoff, R.M., 2012. Animal models of multiple sclerosis: the good, the bad and the bottom line. Nat. Neurosci. 15, 1074–1077.
Rao, S.M., 1995. Neuropsychology of multiple sclerosis. Curr. Opin. Neurol. 8, 216–220.
Rao, S.M., Leo, G.J., Bernardin, L., Unverzagt, F., 1991. Cognitive dysfunction in multiple sclerosis. I. Frequency, patterns, and prediction. Neurology 41, 685–691.
Rossi, S., Furlan, R., De Chiara, V., Muzio, L., Musella, A., Motta, C., Studer, V., Cavasinni, F., Bernardi, G., Martino, G., et al., 2011. Cannabinoid CB1 receptors regulate neuronal TNF-alpha effects in experimental autoimmune encephalomyelitis. Brain Behav. Immun. 25, 1242–1248.
Serra-de-Oliveira, N., Boilesen, S.N., Prado de Franca Carvalho, C., LeSueur-Maluf, L., Zollner Rde, L., Spadari, R.C., Medalha, C.C., Monteiro de Castro, G., 2015. Behavioural changes observed in demyelination model shares similarities with white matter abnormalities in humans. Behav. Brain Res. 287, 265–275.
Stedehouder, J., Couey, J.J., Brizee, D., Hosseini, B., Slotman, J.A., Dirven, C.M.F., Shpak, G., Houtsmuller, A.B., Kushner, S.A., 2017. Fast-spiking parvalbumin interneurons are frequently myelinated in the cerebral cortex of mice and humans. Cereb. Cortex 27, 5001–5013.
Sun, J.J., Ren, Q.G., Xu, L., Zhang, Z.J., 2015. LINGO-1 antibody ameliorates myelin impairment and spatial memory deficits in experimental autoimmune encephalomyelitis mice. Sci. Rep. 5, 14235.
Taylor, L.C., Gilmore, W., Ting, J.P., Matsushima, G.K., 2010. Cuprizone induces similar demyelination in male and female C57BL/6 mice and results in disruption of the estrous cycle. J. Neurosci. Res. 88, 391–402.
Watkins, T.A., Emery, B., Mulinyawe, S., Barres, B.A., 2008. Distinct stages of myelination regulated by gamma-secretase and astrocytes in a rapidly myelinating CNS coculture system. Neuron 60, 555–569.
Xu, H., Yang, H.J., Zhang, Y., Clough, R., Browning, R., Li, X.M., 2009. Behavioral and neurobiological changes in C57BL/6 mice exposed to cuprizone. Behav. Neurosci. 123, 418–429.
Ziehn, M.O., Avedisian, A.A., Tiwari-Woodruff, S., Voskuhl, R.R., 2010. Hippocampal CA1 atrophy and synaptic loss during experimental autoimmune encephalomyelitis, EAE. Lab. Investig. 90, 774–786.